Electronic Supplementary Material (ESI) for RSC Advances.

Simple Tailoring Fabrication of Cu_2O Nanostructures and Their Corresponding Adsorption Ability

Xing Wang, Meizhen Gao*, Xuejian Huo, Elisee Muhire

Key Laboratory for Magnetism and Magnetic Materials of MOE, School of Physical Science and Technology, Lanzhou University, 730000 Lanzhou, China

**Corresponding author. E-mail: gaomz@lzu.edu.cn; Tel: +86 931 8914160*

The concentration of MO is recorded by the UV-Vis spectrum, which can be obtained through Bee-Lambert law in which the absorbance for MO versus concentration obeys a linear relationship at low concentration of MO as shown in **Fig. S1**. The adsorbance of MO (q_t, mg g^{-1}) at time t was calculated using the following formula [Eq. (1)]:

$$q_t = \frac{(C_0 - C_t) \times V}{m} \quad (1)$$

Where C_0 (mg L^{-1}) and C_t (mg L^{-1}) are the initial and final concentration of MO at time t, V (mL) is the volume of the solution and m (mg) is the mass of Cu_2O.

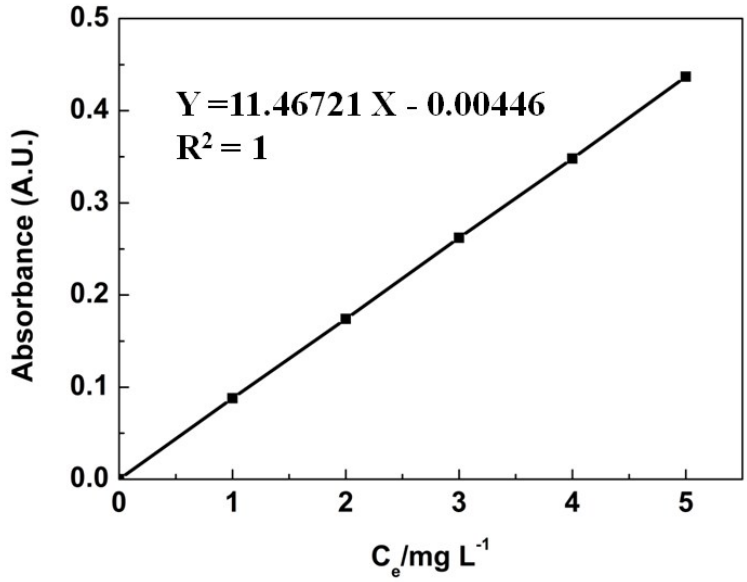

Figure S1. The standard curve of MO solution.

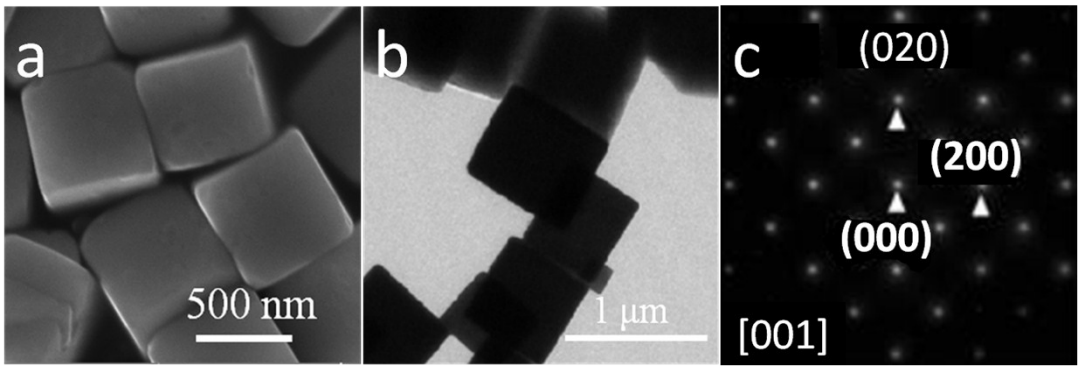

Fig. S2 The detailed structure analysis of the Cu_2O cube.

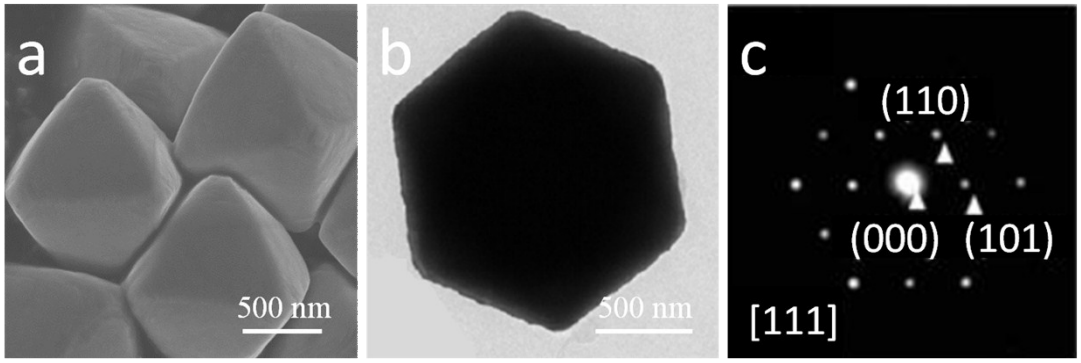

Fig. S3 The detailed structure analysis of the Cu_2O octahedron.

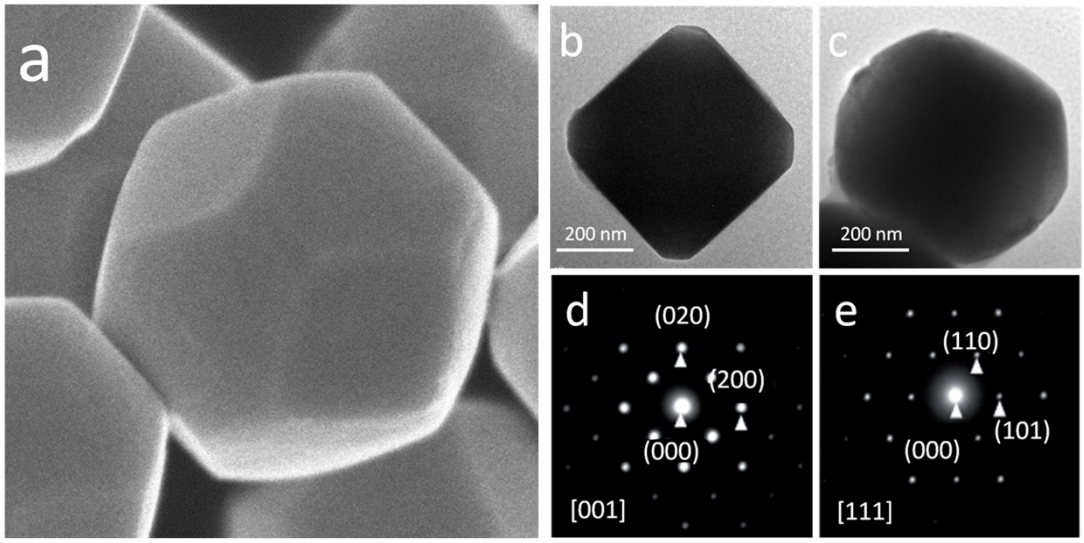

Figure S4. The detailed structure analysis of the Cu_2O cubooctahedron.

As for a cubic structure in **Fig S2**, the exposed surfaces are made of six {100} facets.

If the electron beam is aligned to be perpendicular to {001}, a two-dimensional (2-D) square-shaped projection will be observed. For octahedral structures as depicted in **Fig. S3**, viewed along [110] zone axis, the projection drawing of the octahedron is a parallelogram made of the projections of four {111} facets. **Fig. S4a** shows the SEM of a signal cubooctahedron Cu_2O. **Fig. S4b** shows the TEM of cubooctahedron when the electron beam is aligned to be perpendicular to {001}, a two dimensional square-shaped projection is observed. **T**he corresponding SAED is shown in **Fig. S4d**. With [111] as the viewing direction, the projection changes into an equilateral hexagon constructed by the edges of [100] and [111] (**Fig. S4c**). The corresponding diffraction pattern is shown in **Fig. S4e**.

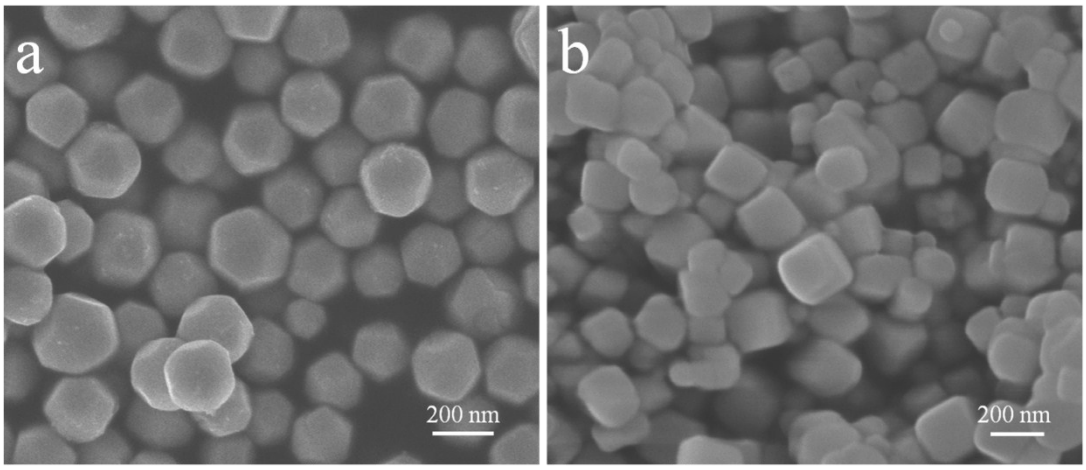

Figure S5. SEM images of Cu_2O nanostructures synthesized at different conditions: all the concentration of NaOH is 0.6 M, (a) cubooctahedrons: the volume of solvent is 60 mL, (b) cubes: the volume of solvent is 150 mL.

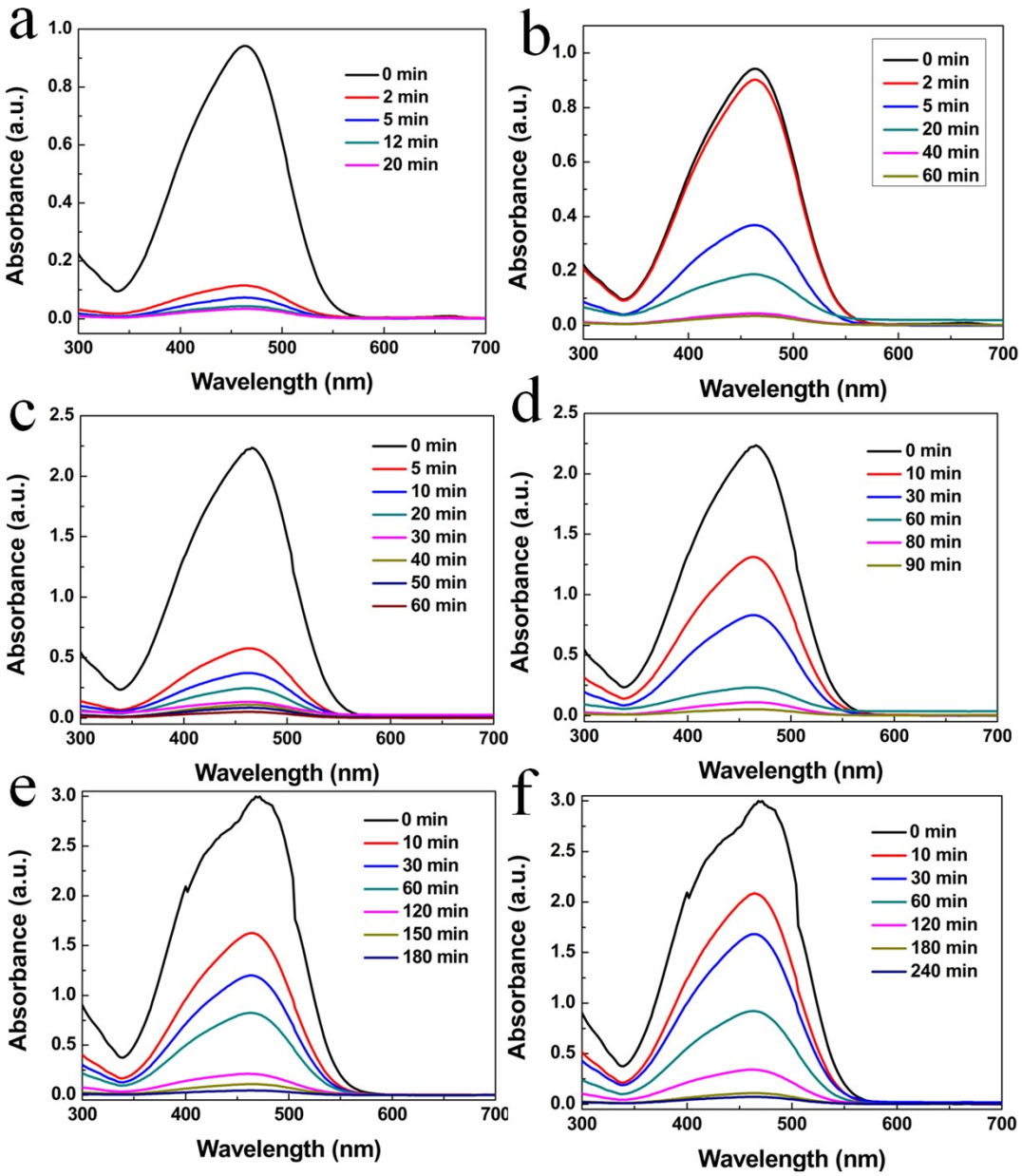

Figure S6. a), c) and e): adsorption spectra of the MO solution in the presence of hollow Cu_2O. **b), d) and f)**: adsorption spectra of the MO solution in the presence of octahedron Cu_2O. (a) and b) 15 mg/L, c) and d) 30 mg/L, e) and f) 50 mg/L)

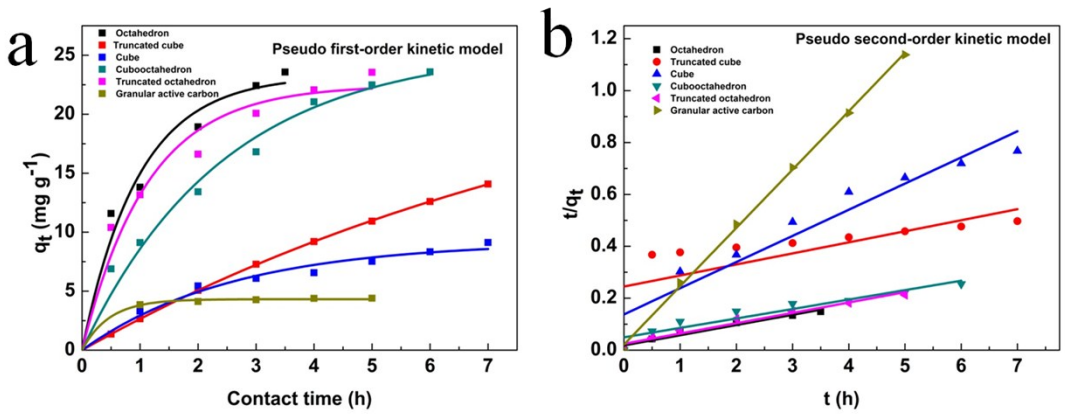

Figure S7. Adsorption kinetics of methyl orange on Cu_2O with different geometries, a) pseudo-first-order kinetic plots, and b) pseudo-second-order plots.

Table S1

The kinetic parameters obtained from IPD fitting on the adsorption process for Cu_2O with different geometries

Pseudo-first order	q_e (mg g^{-1})	k_1 (h^{-1})	R^2
cube	9.2	0.24	0.97532
Truncated cube	28.02	0.38	0.99997
Cubooctahedron	25.54	0.41	0.98202
Truncated octahedron	22.46	0.89	0.96344
Octahedron	23.77	1.03	0.9703
Granular active carbon	4.31	2.15	0.99734
Pseudo-second order	q_e (mg g^{-1})	k_2 (h^{-1})	R^2
cube	9.92	0.01	0.90421
Truncated cube	23.48	0.01	0.43993
Cubooctahedron	27.53	0.03	0.89343
Truncated octahedron	25.15	0.06	0.95881
Octahedron	25.39	0.09	0.94373
Granular active carbon	4.45	2.35	0.99856

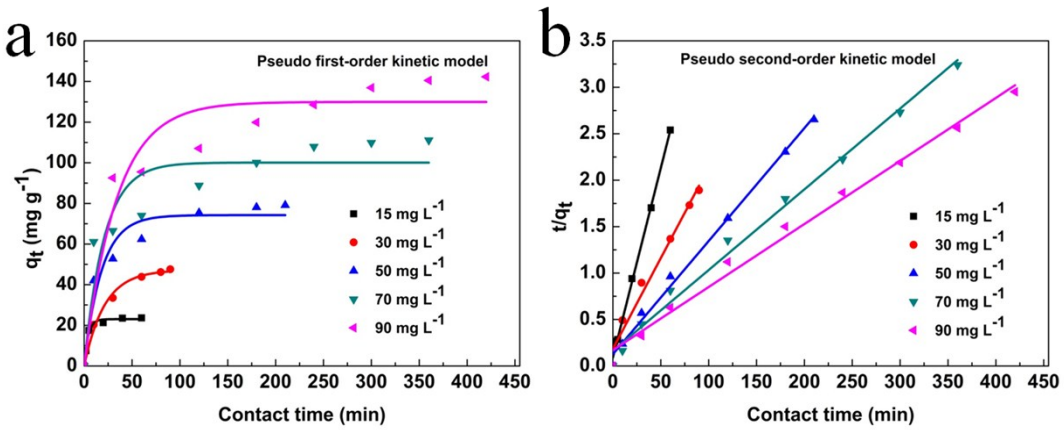

Figure S8. Adsorption kinetics of methyl orange on small octahedral Cu_2O, a) pseudo-first-order kinetic plots, and b) pseudo-second-order plots.

Table S2

The kinetic parameters obtained from IPD fitting on the adsorption process for Cu_2O with small octahedron

Pseudo-first order	15 mg L^{-1}	30 mg L^{-1}	50 mg L^{-1}	70 mg L^{-1}	90 mg L^{-1}
q_e (mg g^{-1})	22.99	47.18	74.23	100.08	129.95
k_1 (min^{-1})	0.245	0.047	0.055	0.048	0.030
R^2	0.9825	0.96992	0.92755	0.83689	0.91394
Pseudo-second order	15 mg L^{-1}	30 mg L^{-1}	50 mg L^{-1}	70 mg L^{-1}	90 mg L^{-1}
q_e (mg g^{-1})	23.65	51.26	82.17	115.07	146.63
k_2 (min^{-1})	0.018	0.001	0.001	0.0005	0.0003
R^2	0.99526	0.99427	0.9935	0.99429	0.99

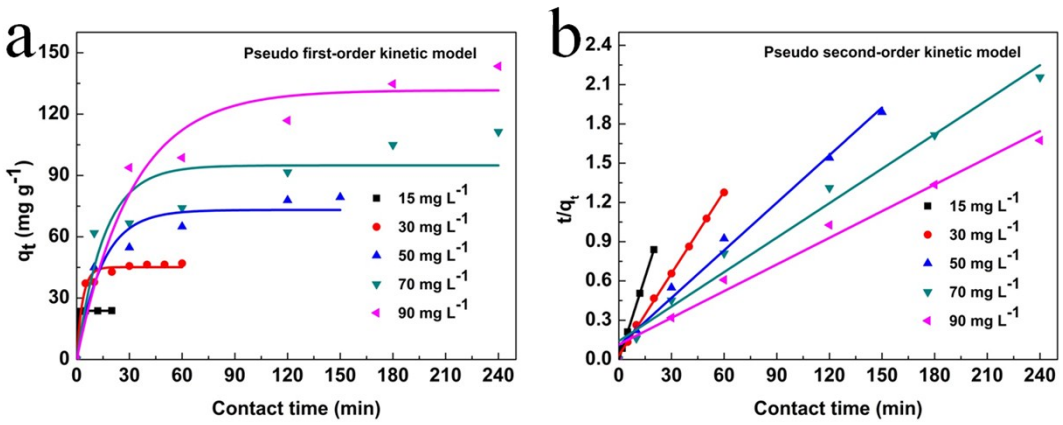

Figure S9. Adsorption kinetics of methyl orange on hollow sphere Cu_2O, a) pseudo-first-order kinetic plots, and b) pseudo-second-order plots.

Table S3

The kinetic parameters obtained from IPD fitting on the adsorption process for Cu_2O with hollow sphere

Pseudo-first order	15 mg L^{-1}	30 mg L^{-1}	50 mg L^{-1}	70 mg L^{-1}	90 mg L^{-1}
q_e (mg g^{-1})	23.79	45.12	73.11	94.89	131.66
k_1 (min^{-1})	2.197	0.296	0.0698	0.065	0.032
R^2	0.99999	0.97212	0.92295	0.8227	0.94033
Pseudo-second order	15 mg L^{-1}	30 mg L^{-1}	50 mg L^{-1}	70 mg L^{-1}	90 mg L^{-1}
q_e (mg g^{-1})	23.87	47.85	82.51	113.9	147.28
k_2 (min^{-1})	1.35	0.014	0.001	0.0005	0.0004
R^2	0.99999	0.99843	0.98777	0.97915	0.97821

Weber and Moris's intraparticle diffusion model also can show the intraparticle diffusion resistance affecting adsorption, which is presented as follows:

$$q_t = k_{ip} t^{1/2} + C_i$$

Where C_i is a constant related to thickness and boundary layer (mg g^{-1}), k_{ip} is the diffusion rate constant (mg g^{-1} $s^{-1/2}$) [1]. The q_t versus $t^{1/2}$ plots for cubic, truncated cubic, cubooctahedral, truncated octahedral and octahedral Cu_2O structures show three reaction steps in the adsorption process (one typical plot is shown as **Figure S10**). For the first stage, the oblique line represents the surface adsorption of MO onto the Cu_2O which can be attributed to electrostatic attraction between the positively charged surface of Cu_2O and the negatively charged MO dye ions. The second line corresponds to intraparticle diffusion process, in which the MO dye ions enter into the inner adsorption sites via the nanoscale channels and adsorb on the surface of ligaments [2]. Finally, the third part is the final equilibrium stage, and the slower intraparticles diffusion lead to the slope close to zero. **Figure S11** list the kinetic parameters of various Cu_2O morphology from the W – M intraparticle diffusion model. K_{d1} and K_{d2} represent the slopes of the first and second adsorption stage respectively, K_{d3} corresponding to the third stage are almost zero and is not listed in Figure 7 and Table S1. It is obvious that the K_{d1} values of cube, truncated cube, cubooctahedron, truncated octahedron and octahedron are gradually increased, which is agreement with the above analysis. And the $K_{d1} > K_{d2}$ is due to that the MO ions compete with each other to penetrate into the nanoscale channels, result in diffusion resistance increasing and diffusion rate at the second stage decreasing [3].

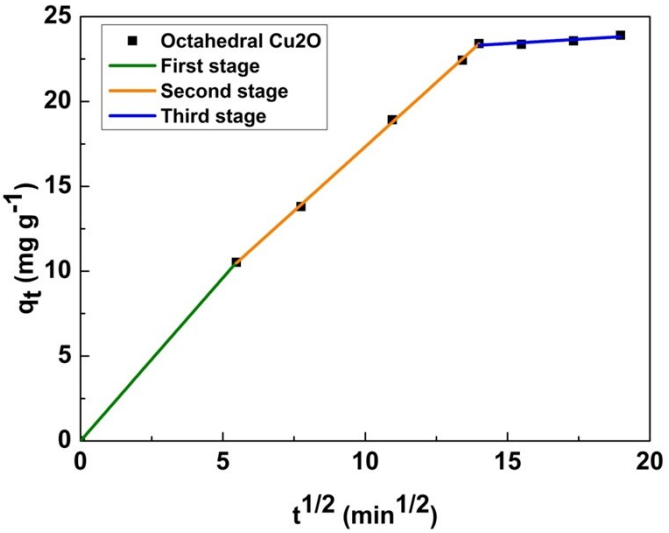

Figure S10. W-M intraparticles diffusion plots for octahedral show three linear correlations over the whole contact time range.

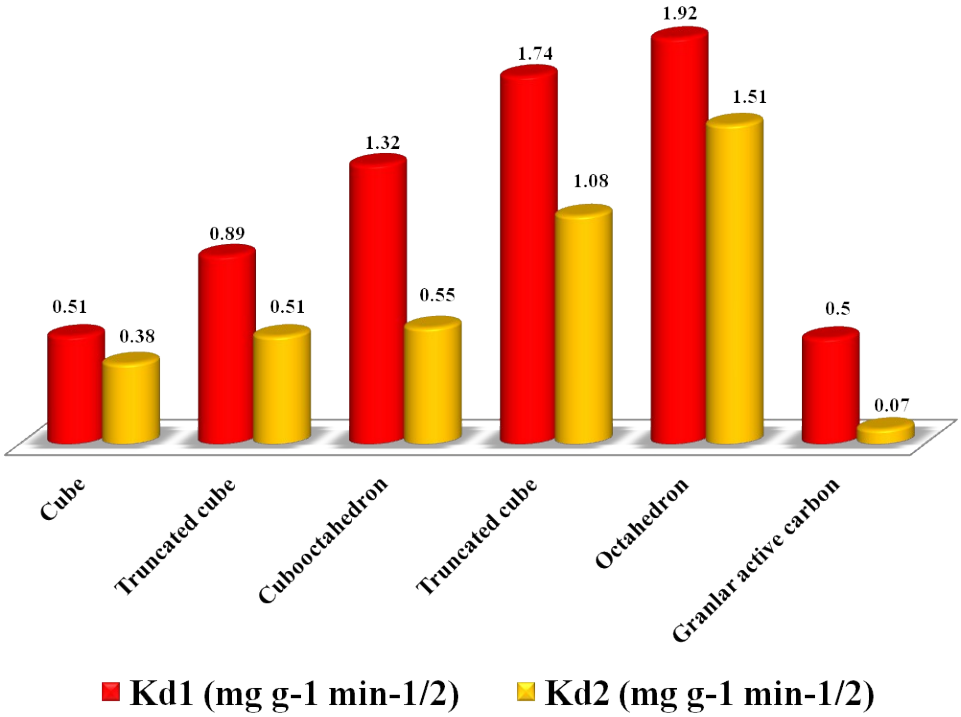

Figure S11. The kinetic parameters histograms for Cu_2O which obtained from W-M intraparticles diffusion model fitting on the adsorption process. K_{d1} and K_{d2} are the slopes of the first and second adsorption stage, respectively.

Table S4

Comparison of adsorption performances based on various Cu_2O microstructures.

Morphology of Cu_2O	MO (mg/L)	Time (min)	Reference
Octahedrons	15	360	[4]
Mesoporous spheres	20	40	[5]
Hollow submicropheres	10	60	[6]
Hollow sphere	15	5	This work

Table S5

Comparison of adsorption performances based on various Cu_2O microstructures.

Morphology of Cu_2O	Ethanol concentration (ppm)	Temperature (℃)	Sensor response	reference
Hollow microspheres	10	240	1.9	[7]
Cubic	50	200	2.64	[8]
Naaanocages	5	210	1.56	[9]
Hollow sphere	1	240	2.36	This work

[1]. K. Wang, X. H. Wu, W. W. Wu, W. Chen, L. Q. Qin, X. M. Cui, Journal of Thermal Analysis and Calorimetry. 2015, 122, 653-663.
[2]. X. Q. Qiao, F. C. Hu, F. Y. Tian, D. F. Hou, D. S. Li, RSC Advance. 2016, 6, 11631-11636.
[3]. E. Demirbas, M. Kobya, M. T. Sulak, Bioresource technology. 2008, 99, 5368-5373.
[4]. D. F. Zhang, H. Zhang, L. Guo, K. Zheng, X. D. Han, Z. Zhang, Journal of Materials Chemistry. 2009, 19, 5220-5225.
[5]. J. L. Liu, Z. Y. Gao, H. J. Han, D. P. Wu, F. Xu, H. X. Wang, K. Jiang, Chemical Engineering Journal. 2012, 185, 151-159.

[6]. X. Q. Ge, H. M. Hu, C. H. Deng, Q. Zheng, M. Wang, G. Y. Chen, Materials Letters. 2015, 141, 214-216.
[7]. H. Zhang, Q. Zhu, Y. Zhang, Y. Wang, L. Zhao, B. Yu, Advanced Functional Materials. 2007, 17, 2766-2771.
[8]. X. J. Wan, J. L. Wang, L. F. Zhu, J. N. Tang, Journal of Materials Chemistry A. 2014, 2, 13641.
[9]. Y. M. Sui, Y. Zeng, W. T. Zheng, B. B. Liu, B. Zou, H. B. Yang, Sensors and Actuators B: Chemical. 2012, 171-172, 135-140.